Journal of Applied Electrochemistry **34**: 1045–1055, 2004.

Cell configurations for performance evaluation in planar solid oxide fuel cells

S.P. JIANG
Fuel Cells Strategic Research Program, School of Mechanical and Production Engineering, Nanyang Technological University, Nanyang Avenue, Singapore 639798
(fax: +65-6791 1859, e-mail: mspjiang@ntu.edu.sg)

Received 2 July 2003; accepted in revised form 20 May 2004

Key words: electrode geometry, electrolyte, reference electrode position, resistance partition, solid oxide fuel cells

Abstract

Cell configurations with asymmetric and symmetric electrode geometries and different reference electrode positions were investigated on 50 mm × 50 mm planar solid oxide fuel cells (SOFC). The reliability and accuracy of the polarization performance of individual electrodes were studied with respect to the electrode geometry and the reference electrode position. The results indicate that a centrally located reference electrode creates inactive electrolyte regions in the center of the cell, pushing the equipotential lines close to the electrode–electrolyte interface region and thus introducing error in the measurement of polarization performance. The potential of reference electrodes located at the corner of the electrode coating was not stable due to the steam build-up in the reference electrode region. Cells with a symmetric electrode geometry arrangement and reference electrodes located at the side of the working electrodes, away from the receiving end of the fuel and oxidant gases, were found to be suitable for performance evaluation in planar SOFC.

1. Introduction

The power output of a solid oxide fuel cell (SOFC) system strongly depends on the performance of the individual cells. This in turn requires accuracy in the determination of various polarization losses. Due to the high operating temperature of about 1000 °C and the all-solid components, the polarization measurement of the individual electrodes of a SOFC are limited by the electrode geometry and the positioning of reference electrodes. Several geometrically different three-electrode configurations have been used to study the electrode reaction and performance on small button-sized disc cells [1–7]. Nagata et al. [3] studied the effect of electrode geometric arrangements on the polarization measurements and showed that overpotential losses of both anode and cathode are related to the position of the reference electrode and the configuration of the working and counter electrodes. This is due to the fact that, as the position of the reference electrode is in the region of nonuniform current density, the reference electrode would sample an average potential in the case of asymmetric electrode configurations. On the other hand, using an internal and Luggin type embedded reference electrode can accurately measure both electrolyte and electrode impedance if the tip of the Luggin is not too close to the working electrode, as demonstrated by Hsieh et al. [7]. However, a Luggin type embedded reference electrode requires a relatively thick electrolyte. For thin electrolyte cells, only external and surface mounted reference electrodes (or pseudoreference electrodes) can be used. There is a lack of information on the electrode geometry requirements and cell configuration for planar SOFC with relatively large electrode area (e.g., 10 cm^2). In the development of SOFC stacking technologies, large planar electrolyte cells were often used to assess the electrode polarization behaviour under simulated stacking conditions such as flow rates, flow patterns and interconnect contact [8–10]. The electrode performance measured on small button cells may not necessarily be the same as the size of the cell increases [11].

In this work, various electrode geometries and cell configurations for the electrode performance evaluation were investigated on planar SOFC with cell dimensions of 50 mm × 50 mm. Stability and reliability of the reference electrode potential and of the electrode performance measurement were studied under fuel cell operation conditions. The results showed that cell configurations with symmetric electrode geometry and reference electrodes positioned at the side of the working electrode and away from the exits of fuel and oxidant gases are suitable for the accurate performance evaluation of planar SOFCs.

2. Experimental details

Yttria-stabilized zirconia (3 mol % Y_2O_3–ZrO_2, Tosoh, Japan) electrolyte plates of 50 mm × 50 mm size were

prepared by tape casting and sintered at 1500 °C for 4 h. The electrolyte thickness was in the range 184 to 247 μm. Strontium doped $LaMnO_3$ (LSM) and 50 vol % Ni/50 vol % Y_2O_3–ZrO_2 (Ni/YSZ) cermet were used as the cathode and anode materials, respectively. They were applied to the electrolyte by screen printing. A LSM cathode and a Ni/YSZ anode were sintered in air for 2 h at 1150 °C and 1400 °C, respectively. Details of preparation of LSM and Ni/YSZ cermet electrodes are given elsewhere [12,13].

Figure 1 shows the cell configurations and gas flow arrangement used. In cell A, a LSM air electrode coating was printed on the entire electrolyte area. The cathode side reference electrode (C_{ref}, also LSM material) was 3 mm × 3 mm in size and was located at the corner. The reference electrode was separated by 2 mm on all sides from the cathode. The fuel electrode coating was centred with respect to the electrolyte. The anode side reference electrode (A_{ref}, also Ni/YSZ cermet material) was 3 mm × 3 mm and was also located at the corner. The gap between the anode reference electrode and anode was 2 mm. Air and fuel reference electrodes were positioned at the opposite sides of the electrolyte and did not form an exact mirror image with respect to their position. This type of electrode arrangement is asymmetric with corner reference electrodes (Figure 1(a)). Cell B was similar to that of cell A except that for cell B, A_{ref} was positioned at the center of the cell. The diameter of the A_{ref} was 3 mm with 2 mm gap between A_{ref} and the anode. Cell B is asymmetric with centrally located A_{ref} (Figure 1(b)).

In cell C, the cathode and anode had the same geometric area and the reference electrodes on both sides were identical, forming a mirror image. The

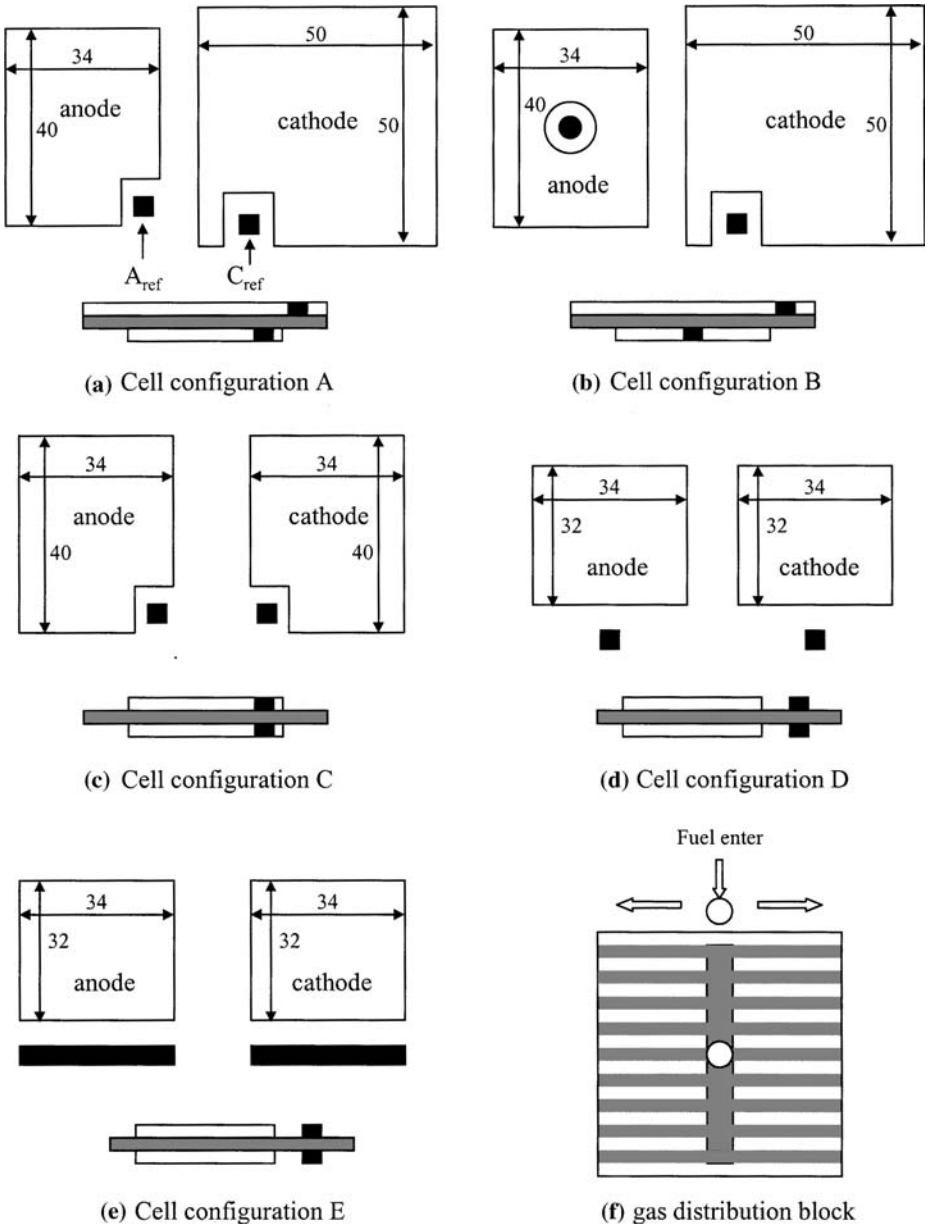

Fig. 1. Schematic diagrams of cell configurations showing the dimension of the electrodes and the relative position of cathode reference (C_{ref}) and anode reference (A_{ref}) electrodes. Gas flows from the centre to the edge of the electrode coating and the numbers are in millimeter.

reference electrode was 3 mm × 3 mm with a 2 mm gap on between the reference and working electrodes. In this arrangement, electrode geometries were symmetric with corner reference electrodes (Figure 1(c)). Electrode arrangements in cells D and E were also symmetric. In contrast to cell C, reference electrodes in cells D and E were located at the side of the working electrodes. The distance between the reference electrode and working electrode was about 5 mm. The dimensions of air and fuel electrodes were 34 mm × 32 mm giving an effective electrode area of about 10.9 cm^2. Reference electrodes in cell D were 4 mm × 3 mm, while in cell E reference electrodes were strip-type with dimension of 34 mm × 3 mm on both sides. Cells D and E were symmetric with side reference electrodes (Figure 1 (d, e)). The position of a reference electrode can also be characterized by an aspect ratio, which is defined as the distance between the reference electrode and the working electrode divided by the electrolyte thickness. For cells A, B and C, the aspect ratio was in the range 8 to 11 while for cells D and E, the ratio was 24 and 27, respectively. In a flat-type geometry, the electrolyte is approximately equipotential at aspect ratios higher than 3 [14]. Table 1 gives details of the cells tested. Current density and cell resistances were calculated based on anode electrode areas. It should be pointed out that the angle of the edge of both electrodes was much small than 90° due to the natural setting of the electrode ink used in the screen-printing process.

Air was used as the oxidant gas and hydrogen, passing through a humidifier (96% H_2/4% H_2O), was used as the fuel. The flow rates of air and hydrogen were controlled by mass flow controllers. Air flow rate was kept constant at 1000 sccm and H_2 flow rates were controlled in the range 400 to 2500 sccm. The gas entered the electrodes through a central hole in an alumina block and was evenly distributed to the porous electrode coating by distribution channels on the block (Figure 1(f)). The alumina block also acted as a support to the electrode.

Ni and Pt woven meshes were used as the current collector on the anode and cathode, respectively. Electrical contacts to the fuel and air side electrodes (including the reference electrodes) were made through Pt wires spot welded to the Ni and Pt meshes. The weight added to the cell was two kilograms. The anode side of the cell was sealed to a metal frame by high temperature glass seals. The assembly was fitted to a polypropylene board to electrically isolate it from the ground. Air and fuel entered the cell through ceramic tubes and there was no contact between the electrodes and the metal frame assembly in order to avoid contamination of the electrodes by chromium species released from the metal frame at high temperatures [15].

Characterization of the electrode polarization behaviour was carried out under fuel cell operation mode, that is, current was drawn from the cell. The electrochemical behaviour of the individual electrodes was measured by galvanostatic current interruption (GCI). With the GCI technique, both overpotential and iR losses can be separated accurately in the time domain [16]. Cells were polarized under 250 mA cm^{-2} at 1000 °C for at least 72 h to reduce the activation effect of the cathodic polarization on the cell performance [17]. Reliability of the cell configuration was monitored by the potential measured between C_{ref} and A_{ref} (P_{ref}) under SOFC operation conditions. Under open circuit, P_{ref} would be expected to be the same as the open circuit potential (V_{ocp}) measured between anode and cathode. The V_{ocp} can be calculated according to the Nernst equation assuming that the ionic transfer number of oxygen ions through the YSZ solid electrolyte is unity [18].

$$V_{ocp} = \left(\frac{RT}{nF}\right) \ln\left(\frac{P'_{O_2}}{P''_{O_2}}\right) \tag{1}$$

where P''_{O_2} is the oxygen partial pressure at the anode, P'_{O_2} the oxygen partial pressure at the cathode, n the number of electrons in the reaction and R, T and F have their usual meanings. In a SOFC such as H_2/H_2O, Pt (anode) |YSZ| (cathode) Pt, O_2, the overall reaction for H_2 oxidation can be written as

$$H_2 + 1/2O_2 = H_2O \tag{2}$$

The standard Gibbs energy, $\Delta G°$ for the reaction is [19]

$$\Delta G° = -246\,602.5 + 54.9\,T \pm 4186.8\ (\mathrm{J}) \tag{3}$$

The oxygen partial pressure, P''_{O_2}, at the anode side can therefore be calculated from the standard Gibbs energy if the ratio of P_{H_2O}/P_{H_2} is known,

$$P''_{O_2} = \left[\frac{P_{H_2O}}{P_{H_2}} \exp\left(\frac{\Delta G^o}{RT}\right)\right]^2 (\mathrm{atm}) \tag{4}$$

Table 1. Details of the cells used

Cell ID	Symmetry and reference electrodes	YSZ thickness	Electrode area/cm^2		Aspect ratio	
		μm	Anode	Cathode	A_{ref}	C_{ref}
A	asymmetric, corner A_{ref} and C_{ref}	247	13.1	24.5	8	8
B	asymmetric, center A_{ref}, corner C_{ref}	186	13.1	24.5	11	11
C	symmetric, corner A_{ref} and C_{ref}	208	13.1	13.1	10	10
D	symmetric, side A_{ref} and C_{ref}	207	10.9	10.9	24	24
E	symmetric, side A_{ref} and C_{ref}	184	10.9	10.9	27	27

Thus, Equation 1 can also be written as

$$V_{ocp} = \frac{RT}{4F}\ln P'_{O_2} - \frac{RT}{2F}\ln\frac{P_{H_2O}}{P_{H_2}} - \frac{1}{2F}\Delta G^{\circ} \quad (5)$$

From the measured P_{ref} value, the water content in the regions close to the anode reference electrodes can also be estimated according to Equation 5 if the P'_{O_2} at the C_{ref} region is assumed to be much less affected under fuel cell operation conditions and is relatively stable. Thus the difference between P_{ref} and V_{ocp} under operating conditions indicates the stability of the reference electrode potential.

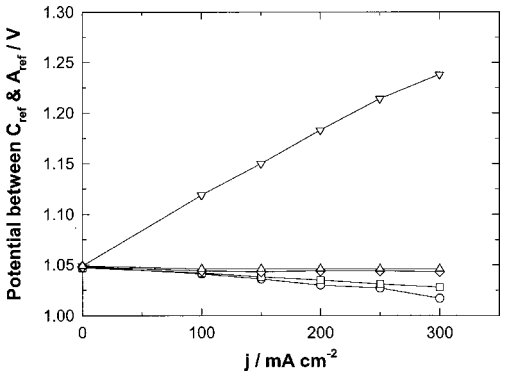

Fig. 3. Steady state potential measured between A_{ref} and C_{ref} under different current densities at 1000 °C. H_2 and air flow rates were 1000 sccm. Key: (○) cell A, (▽) cell B, (□) cell C, (◇) cell D and (△) cell E.

3. Results

Under operating conditions of 96% H_2/4% H_2O and air at 1000 °C, the theoretical V_{ocp} according to Equation 5 is 1.048 V. The measured V_{ocp} of cells at 1000 °C was in the range 1.043 to 1.052 V, very close to the theoretical value under the conditions studied. This indicates good seals and no leakage in the cells tested. Figure 2 shows the cell performance with various cell configurations measured at 1000 °C under hydrogen and air flow rates of 1000 sccm. Some variation in the cell performance can be attributed to variation in the electrolyte thickness and in the fabrication process of individual cells. In cells A and B, the cathode area was 87% larger than the anode area. Nevertheless, cell performance was similar for both asymmetric and symmetric cells, indicating that the extra LSM cathode area in comparison to the anode did not contribute significantly to the overall cell polarization performance.

Under open circuit, P_{ref} was the same as the open circuit potential of the cell. Under operating conditions, P_{ref} may deviate from the V_{ocp} due to changes in the partial pressure of oxygen in regions close to the reference electrodes. Figure 3 shows P_{ref} curves for various cell configurations under different current densities at a H_2 flow rate of 1000 sccm. Cell configuration seems to affect the potential to a fair degree in cells A and C and P_{ref} decreases with increase in current density. In cells D and E, changes in the P_{ref} values were much smaller. The improved stability of the reference electrode potential is most likely related to the side location of the reference electrodes (Figure 1). In cell B, P_{ref} increases with current density, very different from those of other cell configurations in this study. It is noted that cell B is asymmetric with central position of the anode reference electrode (Figure 1(b)).

Figure 4(a) shows the GCI curve of P_{ref} of cell B when a current of 100 mA cm^{-2} was drawn between anode

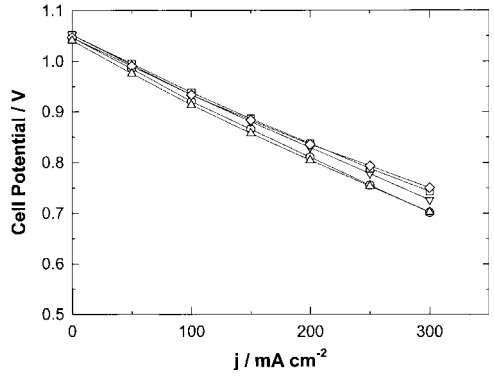

Fig. 2. Cell performance measured at 1000 °C under hydrogen and air flow rates of 1000 sccm. Key: (○) cell A, (▽) cell B, (□) cell C, (◇) cell D and (△) cell E.

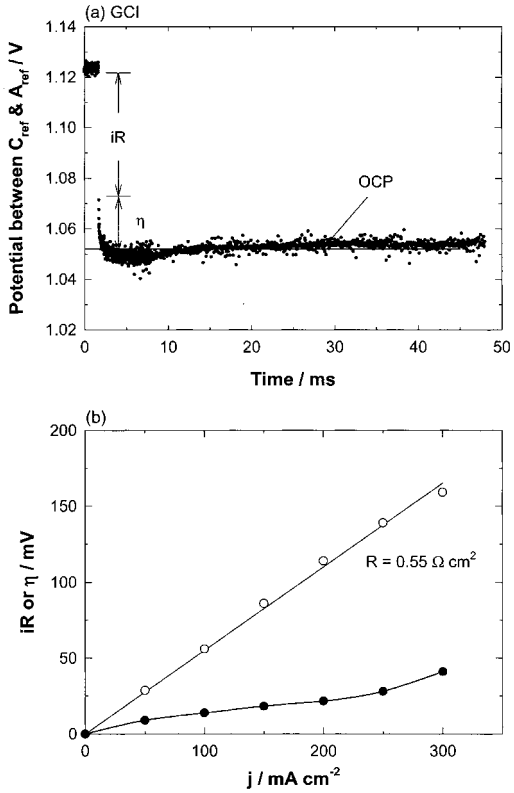

Fig. 4. (a) GCI curves taken between A_{ref} and C_{ref} of the cell B when the cell was operated at 100 mA cm^{-2} and 1000 °C under H_2 and air flow rates of 1000 sccm and (b) the corresponding *iR* (○) and *η* (●) plots.

and cathode at 1000 °C. From the GCI curve, *iR* and overpotential (η) can be clearly identified, similar to that observed on a working electrode. *IR* losses increased linearly with current density and from the slope, a resistance value of 0.55 Ω cm^2 was obtained (Figure 4(b)). The increase in P_{ref} indicates that reference electrode potential is not independent of current density. In the case of other cell configurations, GCI curves of P_{ref} were straight and continuous lines when the cell current was interrupted.

Figure 5 shows the plots of *iR* losses between working electrode (anode and cathode) and reference electrode at 1000 °C and H_2 flow rate of 1000 sccm for cells A, B and E. *IR* curves of cells C and D were similar to that of cell E (Figure 5(c)). Except cell B, *iR* losses measured between anode and C_{ref} were almost the same as that measured between anode and A_{ref} despite the fact that cell A is asymmetric and cells C, D and E are symmetric. Thus, the anode side fraction of electrolyte resistance (R_a) is the same regardless to the use of C_{ref} and A_{ref}. The same is also true for the cathode side fraction of electrolyte resistance (R_c). This indicates that under the conditions studied (e.g., aspect ratio > 8), partition of the electrolyte resistance is independent of the position of the reference electrodes, either on the same or the opposite side of the working electrode. However, in the case of cell B, anode side *iR* measured against C_{ref} is very different from that measured against A_{ref} (Figure 5(b)). R_a was 0.63 Ω cm^2 as measured against A_{ref} and was only 0.09 Ω cm^2 against C_{ref}. The overpotentials measured by A_{ref} and C_{ref} are also very different. For example, at 250 mA cm^{-2}, cathode overpotential (η_c) was 7 mV as measured against A_{ref} and 51 mV against C_{ref}, while anode overpotential (η_a) was 98 and 46 mV as measured against A_{ref} and C_{ref}, respectively. This indicates that electrolyte resistance partition and polarization measurement strongly depend on the position of the reference electrodes in cell B. Table 2 summarises the results of the fractions of electrolyte resistance measured at 1000 °C. In the table, the ratio of the measured cell resistance against A_{ref} and C_{ref} to the calculated electrolyte resistance is also given. The calculated electrolyte resistance was based on the electrolyte thickness and the reported electrolyte resistivity value at 1000 °C [20]. The relatively high measured cell resistance as compared to the calculated electrolyte resistance is related to the constriction phenomena of solid electrolyte cells [8,21,22].

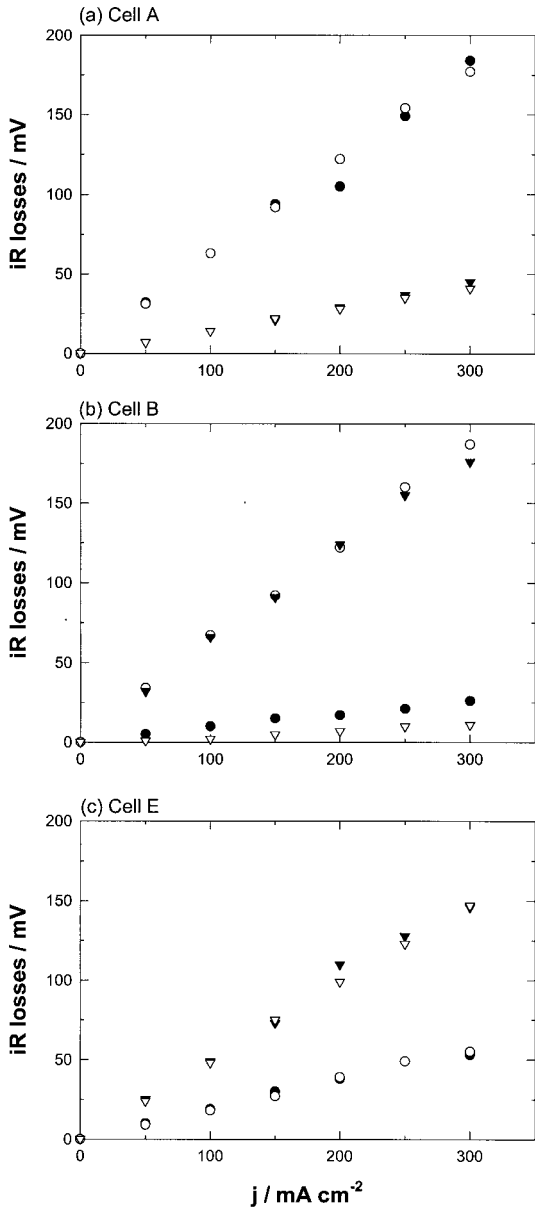

Fig. 5. IR losses between anode, cathode and two reference electrodes at 1000 °C under H_2 and air flow rate of 1000 sccm for cells A, B and E. The *iR* curves of cells C and D were similar to that of cell E. (●) *iR* measured between anode and C_{ref}, (○) *iR* measured between anode and A_{ref}, (▼) *iR* measured between cathode and C_{ref} and (▽) *iR* measured between cathode and A_{ref}.

Figure 6 shows the P_{ref} curves as a function of current density at different H_2 flow rates and 1000 °C under steady state. P_{ref} of cell B is not included due to its very different behaviour (Figures 3 and 5). The H_2 flow rate has a significant effect on the P_{ref} value and the most affected is cell A. For cell A, V_{ocp} was 1.050 V. P_{ref} was reduced to 1.020 V at H_2 flow rate of 800 sccm and 250 mA cm^{-2}, 30 mV lower than the open circuit potential. When the current was increased to 500 mA cm^{-2}, P_{ref} decreased to 0.999 V, 51 mV lower than the open circuit potential. Even at H_2 flow rate of 2000 sccm, P_{ref} was still considerably lower than the open circuit potential. This indicates that the reference electrode potential for cell A is not stable and varies significantly with the H_2 flow rate and current density. Similar variation of P_{ref} was also observed for cell C (Figure 6(b)). In the case of cells D and E, P_{ref} only varied significantly with the current density at low H_2 flow rates (e.g., 500 sccm). When H_2 flow rate was increased to 1000 sccm, P_{ref} was basically independent of the current density and close to the open circuit potential of the cell. The results show that cells D and E produce a much more stable reference electrode potential in comparison to cells A and C, most likely due to the side location of the reference electrodes.

Table 2. Total and fraction of electrolyte resistance measured between anode, cathode, anode reference and cathode reference electrodes at 1000 °C

Cell ID	YSZ thickness	R_{cell}	$R_a/\Omega\ cm^2$		$R_c/\Omega\ cm^2$		R_{cell}/R_{YSZ}	
	/μm	/Ω cm^2	A/C$_{ref}$	A/A$_{ref}$	C/C$_{ref}$	C/A$_{ref}$	A$_{ref}$	C$_{ref}$
A	247	0.75	0.60	0.62	0.14	0.14	1.51	1.47
B	186	0.68	0.09	0.63	0.62	0.03	1.74	1.87
C	208	0.72	0.39	0.40	0.33	0.33	1.72	1.70
D	207	0.64	0.22	0.24	0.40	0.41	1.54	1.47
E	184	0.69	0.19	0.19	0.50	0.49	1.81	1.84

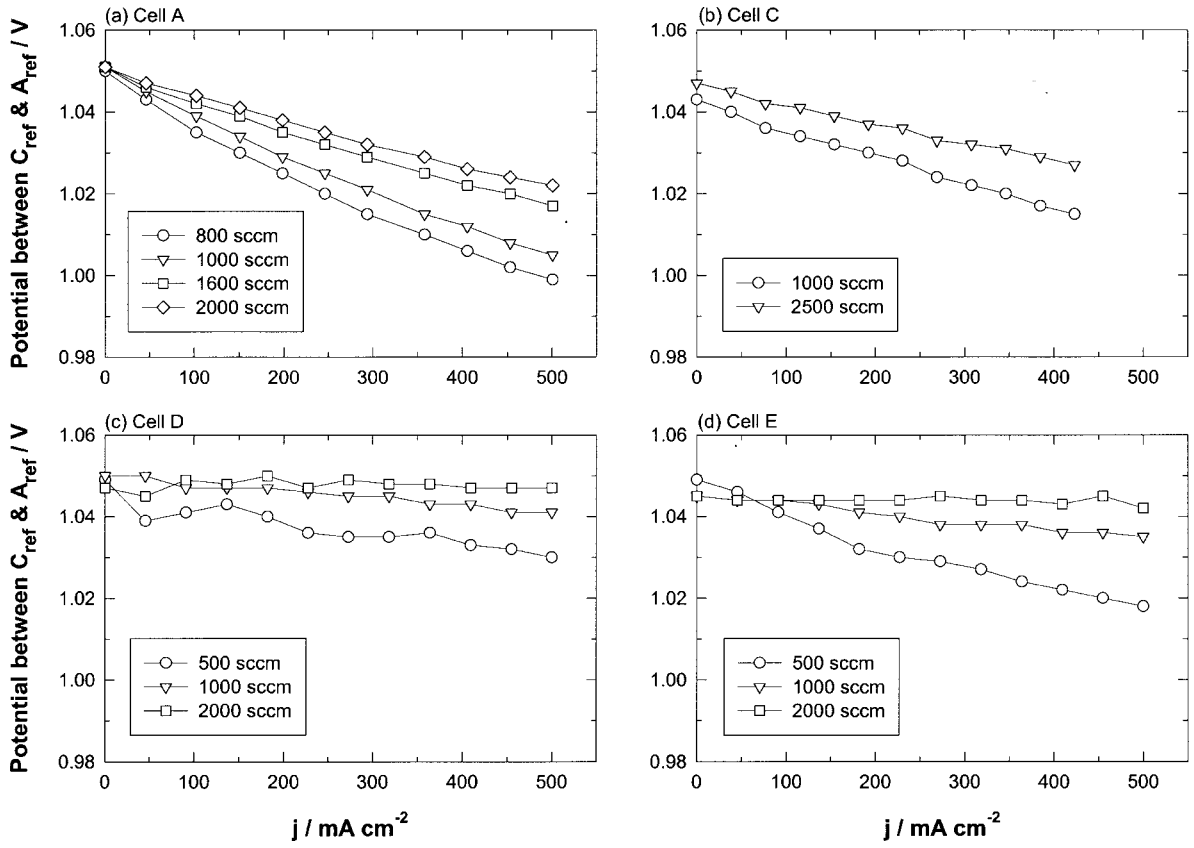

Fig. 6. Steady state potential measured between A$_{ref}$ and C$_{ref}$ (P_{ref}) as a function of current density at 1000 °C and different H_2 flow rates for cells A, C, D and E.

Transitional behaviour of P_{ref} was also investigated under cell operating conditions, as shown in Figure 7 for cell A. The response of P_{ref} strongly depends on the operation conditions. After applying a current density of 250 mA cm^{-2} at 1000 °C and H_2 flow of 400 sccm, P_{ref} instantaneously dropped to 1.003 V and increased slowly to 1.022 V in 40 ms. When the H_2 flow rate was increased to 1000 sccm, the initial P_{ref} value after applying 250 mA cm^{-2} was 1.029 V but reached the open circuit potential within 40 ms. Variation in P_{ref} was also observed for other cell configurations at H_2 flow rate of 500 sccm or lower. At high currents, the response of P_{ref} was slow, resulting in low P_{ref} values (Figure 7(b)). The P_{ref} response shifted in parallel with temperature (Figure 7(c)), indicating that the transitional behavior of P_{ref} may not be thermally activated. As the anode reference electrode was located near the fuel exit, the slow response and low values of P_{ref} as compared to the cell open circuit potential are most likely due to the steam build-up at the anode reference electrode as a result of the water produced (Reaction 2).

Similar transitional behavior of P_{ref} was also observed for cell C as the location of the anode reference electrodes was similar for both cells. In contrast to cells A and C, there was little transitional response of P_{ref} with the current for cells D and E at H_2 flow of 1000 sccm or higher. This again indicates that the cell configurations with side location of reference electrodes produce much stable reference electrode potential as compared to that with corner reference electrodes.

The reliability of the reference electrodes was also investigated by means of overpotential measurement of the electrode reactions at the Ni/YSZ cermet anode and LSM cathode. Figure 8 shows η_a and η_c measured

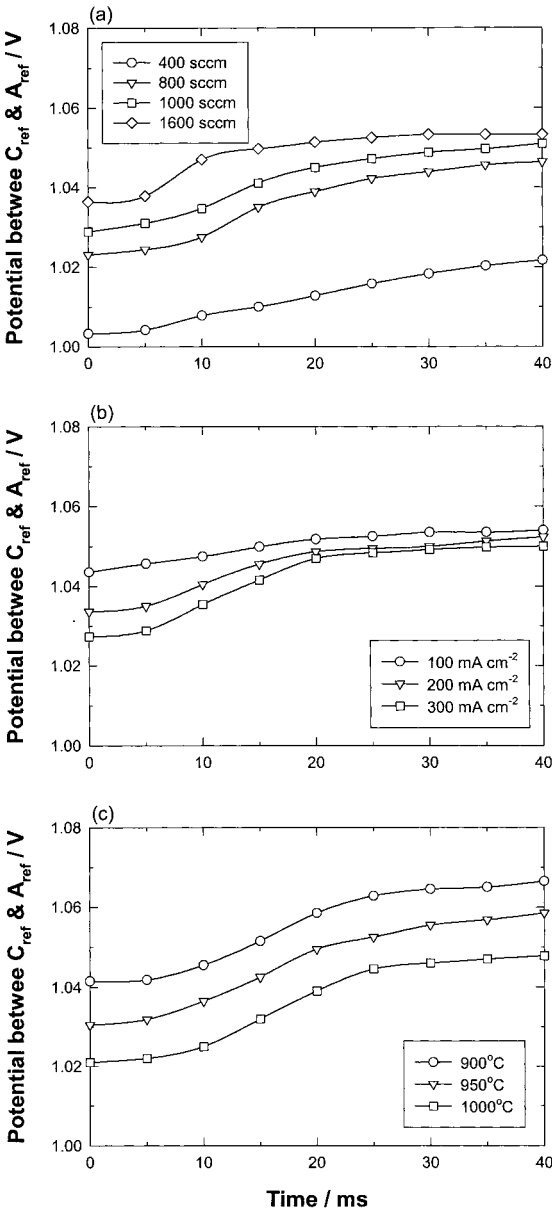

Fig. 7. Transitional behavior of the potential measured between A_{ref} and C_{ref} (P_{ref}) of cell A under various cell operation conditions. (a) effect of H_2 flow rate at 250 mA cm^{-2} and 1000 °C, (b) effect of current density at 1000 °C and H_2 flow rate of 1000 sccm and (c) effect of temperature at 300 mA cm^{-2} and H_2 flow rate of 1000 sccm.

against C_{ref} and A_{ref} and the comparison of the measured and calculated cell potentials for cells A and E at 1000 °C and H_2 flow rate of 1000 sccm. The cell potential (P_{cell}) was calculated according to the following equation.

$$P_{cell} = V_{ocp} - (\eta_a + \eta_c) - j(R_a + R_c) \quad (6)$$

where R_a is the anodic fraction of electrolyte resistance and R_c the cathodic fraction of electrolyte resistance (Figure 5). Overpotential and resistances were measured by C_{ref} or A_{ref}. In the case of cell A, the cell overpotentials ($\eta_a + \eta_c$) measured using A_{ref} were lower than that measured using C_{ref}. Thus the calculated P_{cell} based on overpotentials from A_{ref} was higher than the

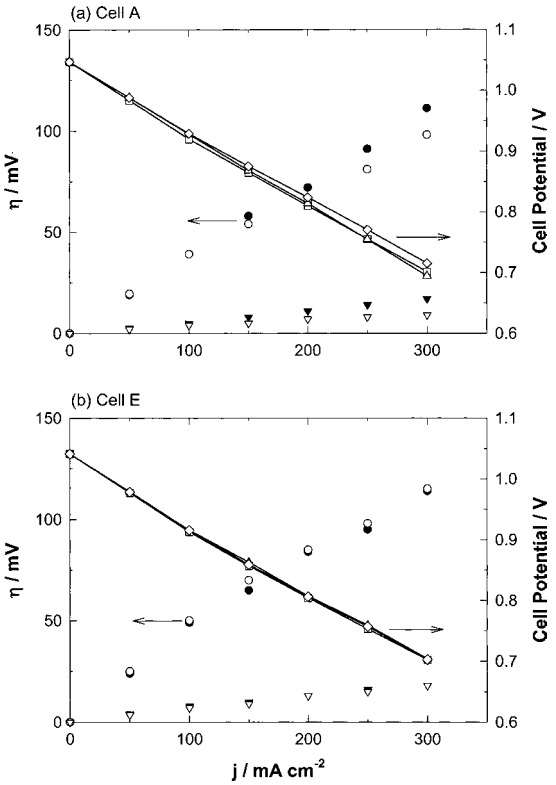

Fig. 8. η_a and η_c measured against C_{ref} and A_{ref} and the comparison of the measured cell potential (P_{cell}) and those calculated based on the measured *iR* and η losses for cells A and E at 1000 °C and H_2 flow rate of 1000 sccm. (●) η_a against C_{ref}, (○) η_a against A_{ref}, (▼) η_c against C_{ref}, (▽) η_c against A_{ref}, (□) measured P_{cell}, (△) calculated P_{cell} based on the measurements against C_{ref} (◇) calculated P_{cell} based on the measurements against A_{ref}.

measured value. On the other hand, the fraction electrolyte resistance values were independent of the reference electrodes used (Table 2). This indicates that the overpotential values measured against A_{ref} are underestimated, thus giving higher electrode performance than the actual one. For cell E, both C_{ref} and A_{ref} gave identical overpotential values and the calculated cell potential is equal to the measured cell potential. This demonstrates the suitability of the cell E for the performance evaluation of planar SOFCs. The high overpotential losses of the Ni/YSZ cermet anode are due to the fact that Ni/YSZ cermet anodes used were not in the optimized state [13].

Limitations in the polarization separation in relation to the YSZ electrolyte thickness were observed on cell configuration E. Figure 9 summarizes the relative anodic and cathodic fractions of electrolyte resistance of 50 mm × 50 mm cells with similar LSM cathode and Ni/YSZ cermet anode as a function of YSZ electrolyte thickness. The cells were tested at 1000 °C or 900 °C under similar conditions as described in this study. In general, R_a is smaller than R_c even though the geometric area of both Ni/YSZ cermet anode and LSM cathode is the same. This is most likely due to the fact that the actual interfacial contact area between Ni/YSZ cermet anode and YSZ electrolyte is higher than that between LSM and YSZ due to the extension of the YSZ phase in

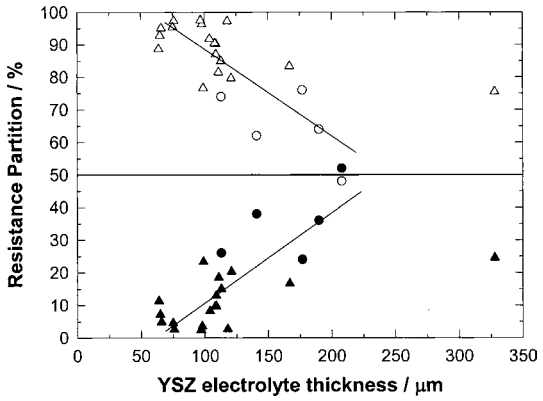

Fig. 9. Relative anodic (R_a) and cathodic (R_c) fractions of electrolyte resistance of 50 mm × 50 mm cells with LSM cathode and Ni/YSZ cermet anode as a function of YSZ electrolyte thickness. Lines are for the guide only. (●) R_a at 1000°C, (O) R_c at 1000 °C, (▲) R_a at 900 °C and (△) R_c at 900 °C.

the Ni/YSZ cermet [23]. As the electrolyte thickness decreases, R_a becomes smaller as compared to R_c. As the fractions of electrolyte resistance are indications of the location of the equipotential lines sampled by the reference electrodes [7], the smaller value of R_a indicates that the equipotential line may shift closer to the anode/electrolyte interface as the electrolyte thickness decreases. At certain points, the separation of the polarization potential would become difficult or impossible. Figure 10 shows an example of polarization curves of two cells with similar LSM cathode and Ni/YSZ cermet anode, measured at 900 °C. Thickness of YSZ electrolyte of these two cells was about 100 μm. Overall performances of these two cells were similar. However, the electrolyte partition of these two cells was quite different. R_a was 24% and 4% for cell 1 and cell 2, respectively. In the case of cell 1, anodic polarization was reasonably separated from the overall polarization potential (Figure 10(a)). For example, at 250 mA cm^{-2}, η_a was 44 mV and close to the 38 ± 11 mV for the H_2 oxidation on Ni/YSZ cermet anodes measured on small cells with electrolyte thickness of about 1 mm and electrode area of about 0.44 cm^2 under similar experimental conditions. In the case of cell 2 (R_a was 4% only), η_a was negligibly small (e.g., only 4 mV at 250 mA cm^{-2}) and η_c was almost the same as the overall cell polarization potential (Figure 10(b)). This indicates that anodic polarization is no longer separable from the overall cell polarization and this is particularly the case for the thin electrolyte cells [24]. The significant variation in the electrolyte resistance partition as shown in Figure 9 probably indicates that the electrolyte resistance partitioning not only depends on the interfacial contact [21–23] but also the contact between the electrode and current collector [8].

4. Discussion

Fractions of the electrolyte resistance are indications of the location of effective equipotential lines sampled by

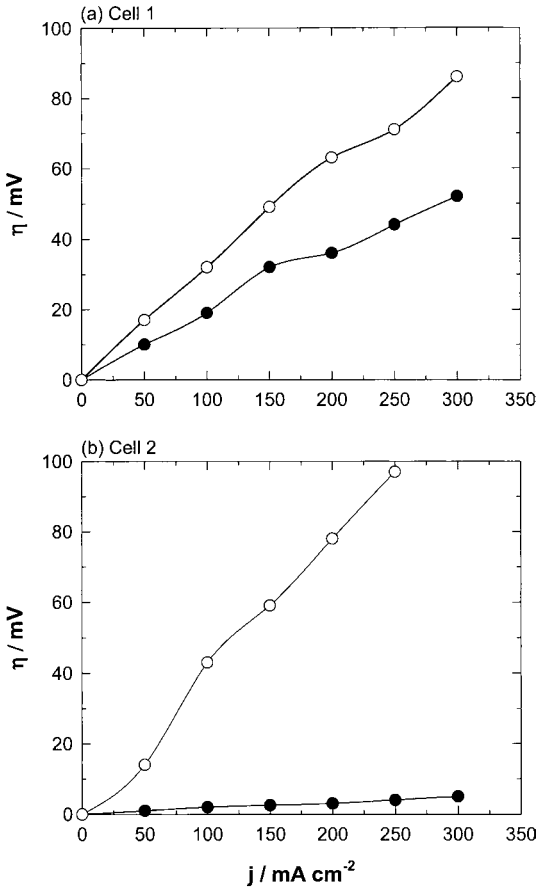

Fig. 10. Polarization curves of (a) cell 1 where $R_a = 0.14\ \Omega\ cm^2$ (24%) and $R_c = 0.44\ \Omega cm^2$ (76%) and (b) cell 2 where $R_a = 0.02\ \Omega\ cm^2$ (4%) and $R_c = 0.54\ \Omega\ cm^2$ (96%). YSZ electrolyte thickness of both cells was about 100 μm and the measurement was made at 900 °C. (●) η_a and (O) η_c.

the anode and cathode reference electrodes in the cells studied (Table 2). In cell A, the cathode is 87% larger than that of the anode and the position of C_{ref} and A_{ref} is not symmetric. Despite the asymmetric arrangement of both working and reference electrodes, the electrolyte resistance partitioning is the same regardless of the reference electrodes used. R_a was 0.6 $\Omega\ cm^2$ when measured against C_{ref}, very close to 0.62 $\Omega\ cm^2$ when measured against A_{ref}. The same is also for the R_c value. In symmetric cells C, D and E, the electrolyte resistance partitioning is also the same regardless of the reference electrodes used, similar to the asymmetric cell A (Table 2). This indicates that under the conditions studied, the equipotential line or surface measured by the reference electrode is independent of the position of the reference electrode. Figure 11(a) shows schematically the location of equipotential line or surface sampled by C_{ref} and A_{ref} electrodes for cell E. A similar location of equipotential line can also be drawn for cells A, C and D. As shown in Figure 11(a), there is no current flow in the electrolyte region between A_{ref} and C_{ref}. P_{ref} measured would be the same as or close to the open circuit potential of the cell under fuel cell operation conditions. This is just the case as shown in Figure 6 at H_2 flow rate higher than 500 sccm.

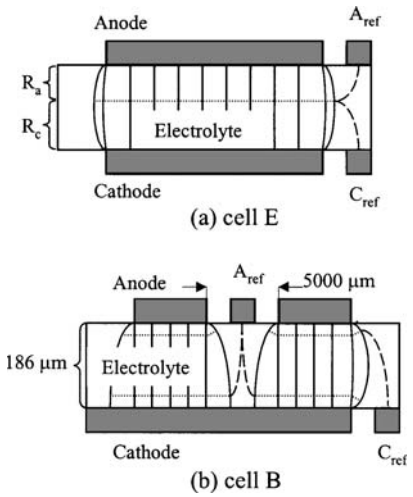

Fig. 11. Schematic diagrams of electric flux distribution and location of equipotential lines sampled by A_{ref} and C_{ref} for (a) cell E and (b) cell B.

In contrast, the fractions of the electrolyte resistance are dependent on the reference electrode in cell B (Table 2). R_a was 0.09 Ω cm^2 with C_{ref} while it was 0.63 Ω cm^2 with A_{ref}. Similarly, R_c measured by A_{ref} was 0.03 Ω cm^2 and was 0.62 Ω cm^2 when measured against C_{ref}. As R_c measured by A_{ref} was only 4% of the overall electrolyte resistance (0.68 Ω cm^2), the equipotenital line sampled by A_{ref} would be very close to the LSM cathode–electrolyte interface. For the same reason, the equipotential line sampled by C_{ref} would be very close to the anode–electrolyte interface. C_{ref} and A_{ref} in cell B measure different equipotential lines. The shift of the equipotential lines to the electrode–electrolyte interface is most likely due to the central position of the anode reference electrode. The diameter of the center open space for A_{ref} was 5000 μm, much larger than the electrolyte thickness of 186 μm. This effectively creates an asymmetry between anode and cathode at the centre region of the cell. As shown by Jiang et al. [25], in the case of thin electrolyte cells, the extension of the region in the electrolyte through which in-plane ionic current may flow due to the asymmetry between anode and cathode would be very small and can be ignored. This would result in the existence of an electrically neutral or inactive region between anode and cathode in the center of the cell where there is no ionic current flow under cell operation conditions. The neutral region in the electrolyte between anode and cathode could push the equipotential line to the region close to the electrode–electrolyte interface. This is confirmed by the very small R_c and R_a values as measured by A_{ref} and C_{ref}, respectively. Figure 11(b) shows the electric field and the location of equipotential lines sampled by C_{ref} and A_{ref} in cell B. It shows that P_{ref} measured between C_{ref} and A_{ref} would be the open circuit potential plus the electrolyte contribution due to the electric flux between these two reference electrodes. This explains the observation that P_{ref} increased with current density (Figure 3). From the GCI measurement, the electrolyte portion involved in P_{ref} is about 0.55 Ω cm^2 (Figure 4), about 81% of the overall electrolyte resistance. The central location of reference electrodes introduces electrode asymmetry and creates an electrolyte region in the centre of the cell where there is no ionic current flow. This could distort the electric flux and force the equipotential lines close to the electrode–electrolyte interface region, introducing error in the polarization measurement of individual electrodes. Thus, the location of equipotenital lines close to the electrode–electrolyte interface is the main reason for the observed significant difference in overpotentials measured against A_{ref} and C_{ref}. In conclusion, cell configuration with the central location of reference electrodes is not recommended for performance evaluation in thin electrolyte cells.

The steady state P_{ref} values are significantly affected by the operating conditions such as current density and H_2 flow rates particularly for cells with corner reference electrodes (cells A and C) (Figure 6). As air flow rate was kept constant at 1000 sccm and there was no seal to the LSM cathode side, the effect of the depleted air due to the oxygen reduction reaction on the partial pressure of oxygen at the cathode reference electrode region would be very small and negligible. Thus the change in P_{ref} is primarily due to the change of the partial pressure of oxygen at the anode reference electrode area as the result of the steam build-up (Figure 6). As A_{ref} was located at the corner (i.e., the edge) of the electrode coating, the decrease in P_{ref} is an indication of the increase in water content in the H_2 fuel travelling from the centre to the edge of the electrode coating (Figure 1(f)). Figure 12 shows the initial input H_2O% at the center and H_2O% at the edge of the electrode coating at different current densities and H_2 flow rates for cell A at 1000 °C. The initial water content at the centre of the coating was 3.75% based on the observed V_{ocp} of 1.050 V. H_2O content in H_2 at the edge of the anode was calculated based on the P_{ref} values of Figure 6(a)

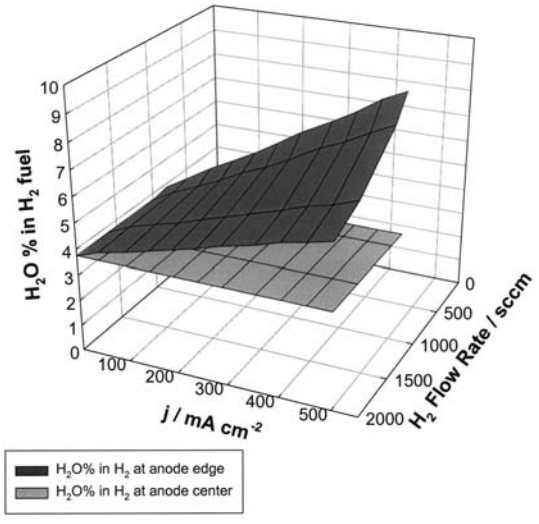

Fig. 12. Water content in the H_2 fuel at the center and the edge of cell A as a function of current density and H_2 flow rates at 1000 °C.

according to Equation 5. The water content at the edge of the electrode coating (i.e., the A_{ref} region) was considerably higher. For example, at a current density of 500 mA cm^{-2} and H_2 flow rate of 800 sccm, the H_2O content in H_2 was 9.2% at the edge of the electrode, about 5% higher than that in the centre of the electrode. Even at normal operation current density of 250 mA cm^{-2}, the H_2O content at the edge of the electrode coating was 6.5%. Such a significant increase in the water content in H_2 occurred in a fuel flow distance of about 14 mm (Figure 1(f)). This indicates that for planar cells with long flow channels, the accumulated water content at the fuel exit regions can be substantial and excess water content can lead to the reduction in the polarization performance of Ni/YSZ based cermet anodes [9,26]. Therefore, fuel flow channel length should be designed as short as practical to prevent flooding of the electrode at the exit regions of the cell.

Transitional response of P_{ref} for cells A and C also strongly depends on the operating conditions (Figure 7). The observations of the unsteady behavior of P_{ref} for cells A and C clearly demonstrate that considerable steam can build up near the anode reference electrode located at the corner of the electrode coating particularly at high current and low flow rates, resulting in the instability in the reference electrode potential. The instability of the anode reference electrode potential can, in fact, reduce the accuracy of the polarization performance measurement (Figure 8). However, for cells D and E with anode reference electrodes located at the side of the working electrodes, the effect of the current density and H_2 flow rate on steady state and transitional P_{ref} behaviour was very small for H_2 flow rates higher than 500 sccm (Figure 6 (c,d)), indicating very stable reference electrode potentials. Thus the reference electrode should be positioned away from the fuel and air exit to avoid the effect of the change in partial pressure of oxygen of the reactant gases on the reference electrode potential during the operation.

The effect of misalignment between anode and cathode on the current distribution and accuracy of polarization measurements have been analysed theoretically [27–30]. For example, a misalignment of 11% of the electrolyte thickness ($d/L=1/9$ where d is the misalignment between anode and cathode and L is the electrolyte thickness) would create measurable difference and distortion in ohmic resistance and in impedance and polarization responses [28,29]. However, experimental verification of theoretical models is rare. This may be largely due to the fact that accurate alignment of the edges of both electrodes would be hard to achieve in the case of thin electrolyte cells. For example, to achieve $d/L \leqslant 1/9$, the difference in the mutual position of both electrodes should be less than 22 μm in the case of electrolyte thickness of about 200 μm and 11 μm if the electrolyte thickness is reduced to 100 μm. Such accuracy in the fabrication of SOFC electrode coatings would be very difficult to obtain if not impossible with conventional electrode coating techniques. In the cells with screenprinted LSM cathode and Ni/YSZ cermet anodes, the misalignment between electrodes was typically within the region of 0.5 mm. This corresponds to a misalignment of 250% for cells with electrolyte thickness of 200 μm. Nevertheless, the separation of anodic and cathodic overpotentials in cell E is very reasonable. The significance of this study is the direct experimental evidence that the effect of misalignment on the electrochemical characterization of electrode process may be significantly related to the electrolyte thickness and certain misalignment could be tolerated in the case of thick electrolyte cells. The underestimation of anodic polarization due to the large anode would only become problematic for thin electrolyte cells (e.g., for electrolyte cells with thickness <200 μm, see Figures 9 and 10). As shown in Figure 9, there is a trend that the division between R_a and R_c increases significantly with the decrease in electrolyte thickness for cells with electrolyte thickness lower than about 200 μm. The reasons for such tendency are not clear at this stage. One explanation may be related to the increased importance of the contact resistances between electrode and current collector as the electrolyte thickness decreases [8,23].

5. Conclusion

Five cells with asymmetric and symmetric electrode arrangements and various locations of reference electrodes were investigated for the performance evaluation of 50 mm × 50 mm SOFC plate cells. The results of the investigation can be summarized as follows:

(i) A centrally located reference electrode (cell B) can cause an inactive electrolyte region in the centre of the cell and push the equipotential line close to the electrode/electrolyte interface, introducing distortion in the electrode polarization measurement. For cells with corner reference electrodes, the potential of the reference electrodes is not stable primarily due to the significant steam built-up at the anode reference electrode area (cells A and C).

(ii) In cells A, C, D and E, equipotential lines or surfaces sampled by reference electrodes are independent of the position of the reference electrodes. The best cell configurations from this study are one with symmetric electrode arrangement and side location of reference electrodes (cells D and E). A Cell E with strip-type reference electrode is preferred for case of contact between the current collector and the reference electrodes.

(iii) The reliability of symmetric cell configuration such as cells D and E in the measurement of anodic and cathodic polarization potentials in thin electrolyte cells could be assessed by the relative anodic and cathodic partitioning of the electrolyte resistance. A close correlation between the fraction of electrolyte resistance and electrolyte thickness was observed.

Acknowledgement

I would like to thank Dr Y. Ramprakash for the technical contribution and Dr David Butler for valuable comments.

Reference

1. S. Prindahl and M. Mogensen, *J. Electrochem. Soc.* **145** (1998) 2431.
2. D.M. Reed, H.U. Anderson and W. Huebner, *J. Electrochem. Soc.* **143** (1996) 1558.
3. M. Nagata, Y. Itoh and H. Iwahara, *Solid State Ionics* **67** (1994) 215.
4. S.P. Jiang and S.P.S. Badwal, *J. Electrochem. Soc.* **144** (1997) 3777.
5. J. Divisek, L.G.J. de Haart, P. Holtappels, T. Lennartz, W. Malléner, U. Stimming and K. Wippermann, *J. Power Sources* **49** (1994) 257.
6. A. Khandar, S. Elangovan and M. Liu, *Solid State Ionics* **52** (1992) 57.
7. G. Hsieh, T.O. Mason, E.J. Garbozi and L.R. Pederson, *Solid State Ionics* **96** (1997) 153.
8. S.P. Jiang, J.G. Love and L. Apateanu, *Solid State Ionics* **160** (2003) 15.
9. S.P. Jiang and Y. Ramprakash, *Solid State Ionics* **116** (1999) 145.
10. D. Ghosh, G. Wang, R. Brule, E. Tang and P. Huang, *in* S.C. Singhal and M. Dokiya (Eds), SOFC-VI, PV 99-19, The Electrochemical Society, Pennington, NJ (1999), p.822.
11. S.P. Jiang, *J. Power Sources* **124** (2003) 390.
12. S.P. Jiang, J.P. Zhang, Y. Ramprakash, D. Milosevic and K. Wilshier, *J. Mater. Sci.* **35** (2000) 2735.
13. S.P. Jiang, P.J. Callus and S.P.S. Badwal, *Solid State Ionics* **132** (2000) 1.
14. S.B. Adler, B.T. Henderson, M.A. Wilson, D.M. Taylor and R.E. Richards, *Solid State Ionics* **134** (2000) 35.
15. S.P. Jiang, J.P. Zhang, L. Apateanu and K. Foger, *J. Electrochem. Soc.* **147** (2000) 4013.
16. S.P. Jiang, J.G. Love and S.P.S. Badwal, *in* J. Nowotny and C.C. Sorrell (Eds), 'Electrical Properties of Oxide Materials' (Trans. Tech. Publications, 1997), p. 81.
17. S.P. Jiang and J.G. Love, *Solid State Ionics* **138** (2001) 183.
18. S.W. Zha, C.R. Xia and G.Y. Meng, *J. App. Electrochem.* **31** (2001) 93.
19. O. Kubaschewski and C.B. Alcock, 'Metallurgical Thermochemistry' (Pergamon Press, Oxford, UK, 1979), p. 380.
20. F.T. Ciacchi, K.M. Crane and S.P.S. Badwal, *Solid State Ionics* **73** (1994) 49.
21. T. Kenjo and Y. Kanehira, *Solid State Ionics* **148** (2002) 1.
22. J. Fleig and J. Maier, *J. Electrochem. Soc.* **144** (1997) L302.
23. S.P. Jiang, *J. Electrochem. Soc.* **148** (2001) A887.
24. Y.J. Leng, S.H. Chan, K.A. Khor and S.P. Jiang, *J. Appl. Electrochem.* **34** (2004) 409.
25. Y. Jiang, A.V. Virkar and F. Zhao, *J. Electrochem. Soc.* **148** (2001) A1091.
26. K. Eguchi, Y. Kunisa, K. Adachi and H. Arai, *J. Electrochem. Soc.* **143** (1996) 3699.
27. S.H. Chan, X.J. Chen and K.A. Khor, *J. Appl. Electrochem.* **31** (2001) 1163.
28. S.B. Adler, *J. Electrochem. Soc.* **149** (2002) E166.
29. J. Winkler, P.V. Hendriksen, N. Bonanos and M. Mogensen, *J. Electrochem. Soc.* **145** (1998) 1184.
30. J. Fleig and J. Maier, *Solid State Ionics* **94** (1997) 199.